Staggered and extreme localization of electron states in fractal space

Biplab Pal and Arunava Chakrabarti*
Department of Physics, University of Kalyani, Kalyani, West Bengal 741 235, India
(Received 24 April 2012; published 13 June 2012)

We present exact analytical results revealing the existence of a countable infinity of unusual single-particle states, which are localized with a multitude of localization lengths in a Vicsek fractal network with diamond-shaped loops as the "unit cells." The family of localized states forms clusters of increasing size, much in the sense of Aharonov-Bohm cages [J. Vidal *et al*., Phys. Rev. Lett. **81**, 5888 (1998)], but now without a magnetic field. The length scale at which the localization effect for each of these states sets in can be uniquely predicted following a well-defined prescription developed within the framework of a real-space renormalization group. The scheme allows an exact evaluation of the energy eigenvalue for every such state which is ensured to remain in the spectrum of the system even in the thermodynamic limit. In addition, we discuss the existence of a perfectly conducting state at the band center of this geometry and the influence of a uniform magnetic field threading each elementary plaquette of the lattice on its spectral properties. Of particular interest is the case of extreme localization of single-particle states when the magnetic flux equals half the fundamental flux quantum.

DOI: 10.1103/PhysRevB.85.214203 PACS number(s): 71.23.An, 73.20.Fz, 73.22.Dj

I. INTRODUCTION

The interplay of lattice topology and quantum interference effects is known to give rise to an exotic electronic spectrum in solid systems that has been studied in detail for several decades now. The subject is still being pursued with vigor to achieve comprehensive control over coherent transport in low dimensions.

In quantum interference and related transport mechanisms a pivotal role is played by the localization of electronic eigenstates in the presence of disorder. Such a localization, known as the Anderson localization,[1] upholds a central result that, in one dimension with arbitrary disorder, all the single-particle states will be exponentially localized, and the same was shown to be true in two dimensions as well.[2] Since then, extensive research has been undertaken to understand the fundamentals of localization effects, studies ranging from electronic states in random lattice models[3–8] to the Anderson localization of light,[9,10] spin freezing in one-dimensional semiconductors,[11] and localization in optical lattices,[12] to name a few. Matter waves can also be localized in deterministic potentials sharing certain features of random disorder.[13,14] Recent experiments revealed the Anderson localization of noninteracting Bose-Einstein condensates in one-dimensional matter waveguides, where the random potential has been generated by laser speckles.[15] Similar experiments have also been reported to study the Anderson localization in optical lattices[16,17] and in the cases of microwaves[18] and of classical waves in a weakly disordered one-dimensional stack of metamaterials.[19]

Variations of the classic Anderson localization are also well known by now. Isolated delocalized (extended) single-particle states exist, even in a disordered one-dimensional chain of atomic potentials, resulting out of a kind of spatial correlation,[20–22] in one-dimensional quasiperiodic chains,[23–27] or in certain kinds of deterministic fractal geometries.[28–30] Crossovers from an insulating to a metallic spectral behavior in correlated disordered two-legged ladder networks have also been reported recently.[31,32]

A curious point, apparently unnoticed or unappreciated so far, is that, while a precise determination of the eigenvalues corresponding to the extended single-particle states is possible in the above cases of correlated and aperiodic order, the task seems to be practically impossible when it comes to an exact evaluation of eigenvalues of the localized states in a random or even an aperiodically ordered system in the *thermodynamic limit*. It should be appreciated that, although a direct diagonalization of the Hamiltonian for a finite size of the system yields eigenvalues of the localized states (for a disordered or an aperiodically ordered system), there is no *a priori* reason to assume that these eigenvalues remain in the spectrum when the system grows in size and tends to infinity. In fact, for a deterministic fractal geometry that offers a singular continuous spectrum, it is almost impossible to find the exact eigenvalues corresponding to the states that will finally be localized on an infinite lattice. To the best of our knowledge, this issue remains unaddressed so far in the literature.

Can one really identify the localized states and extract the corresponding eigenvalues for an aperiodically ordered system? In this paper we address ourselves this question and take up the task of critically examining the spectral properties of a Vicsek fractal network[33] consisting of *diamond*-shaped loops within a tight-binding formalism. While looking for the localized state eigenvalues and the nature of localization are indeed the major factors driving this work, other interests in such a study are related to the general spectral character and magnetotransport in such systems. The motivation behind the latter part of this work may be summarized as follows. A *diamond-Vicsek* network (see Fig. 1) provides an interesting geometry in which the "open" character of a typical Vicsek pattern is preserved along with the presence of closed loops in shorter scales of length. This is in marked contrast to the much studied Sierpinski gasket,[34,35] which is a closed structure, or to the other open tree fractals[36] or even an alternative version of the Vicsek fractal without any local closed loops.[37] The presence of these loops effectively generates a longer-ranged interaction between the atomic sites occupying the various vertices, and its effect on the electron localization or delocalization is worth studying.

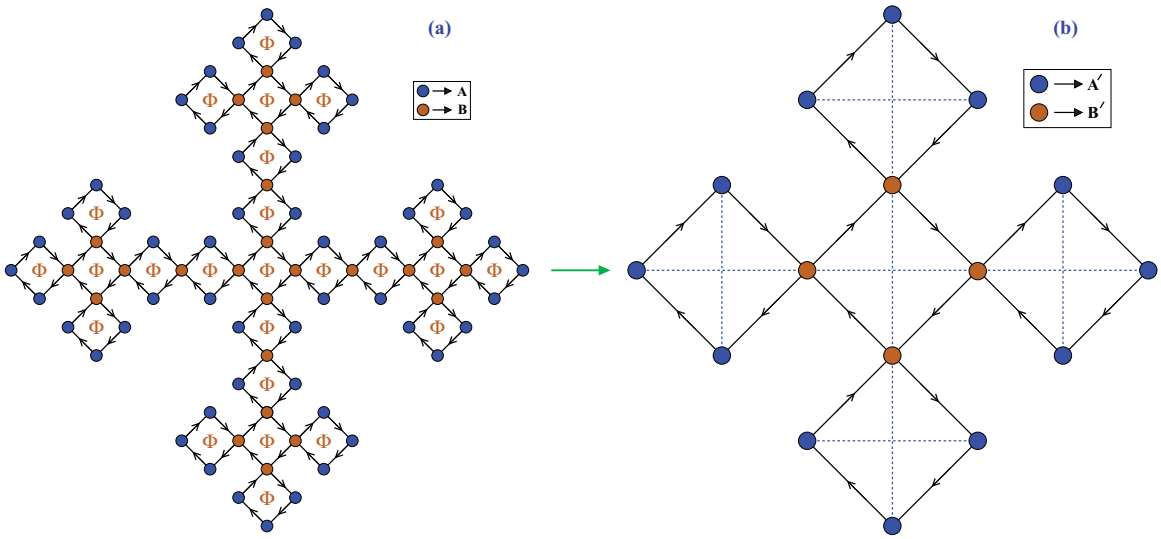

FIG. 1. (Color online) (a) Schematic view of the second generation of an infinite diamond-Vicsek network with each diamond plaquette threaded by a uniform magnetic flux Φ. The edge sites are denoted by A (blue circles), and the bulk sites are denoted by B (orange circles); the arrow indicates the direction of the forward hopping. We exclude any next-nearest-neighbor hopping at the beginning. (b) Renormalized version of (a), with the dotted lines indicating the diagonal hopping which is generated due to renormalization.

Second, linear arrays of diamond networks have already drawn considerable attention in recent years in the context of charge and spin transport properties,[38–40] having been shown to behave as a *flux-controlled* n- or p-type semiconductor,[38] or as a prospective candidate of an elegant spin filter.[39,40] The influence of a topological variation in the arrangement of such loops on the spectral properties of the system is thus worth investigating, both from the standpoint of fundamental physics and from the perspective of device technology. We choose such a deterministic geometry to make an analytical approach to the system possible.

We find extremely interesting results in the context of the localization of electronic states. In the absence of any external magnetic field, a countable infinity of localized states can be precisely detected with a multitude of localization lengths. One can work out an exact mathematical prescription to specify the length scale at which the onset of localization takes place. The localization can, in principle, be *delayed* (staggered) in position space, and the corresponding energy eigenvalues can be exactly evaluated following the same prescription based on a real-space renormalization group (RSRG) method. In addition, it is shown that, for a given set of parameters, the center of the spectrum corresponds to a perfectly extended eigenstate, with the parameters of the Hamiltonian exhibiting a fixed point behavior. Switching on a magnetic field opens up gaps in the spectrum in general and even leads to an extreme localization of all the single-particle states in the sense of the formation of the Aharonov-Bohm cages.[41]

In what follows we describe the results. In Sec. II, the model and the mathematical method of handling the problem are presented. Sections III and IV include the results and their analyses related to the spectral properties without and with the magnetic field, respectively. The two-terminal transport study is carried out in Sec. V, and in Sec. VI we draw our conclusions.

II. THE SYSTEM AND THE MATHEMATICAL FORMULATION

A. The Hamiltonian

We refer to Fig. 1(a), which illustrates the second generation of a Vicsek geometry with diamond-shaped loops. As, at one stage, we shall be considering the effect of a magnetic field on the spectral properties, we show in Fig. 1(a) the flux distribution. Each plaquette is threaded by a uniform magnetic flux Φ. The atomic sites are assigned a different status depending on their positions and neighborhood in the lattice; namely, the sites in the bulk are called B sites, while A sites refer to the sites sitting at the edges. The magnetic field breaks the time-reversal symmetry along the edges of every diamond. The Hamiltonian, in the tight-binding formalism, is written as

$$\boldsymbol{H} = \sum_i \epsilon_i |i\rangle\langle i| + \sum_{\langle ij\rangle} [t_{ij} e^{i\theta_{ij}} |i\rangle\langle j| + t_{ji} e^{-i\theta_{ij}} |j\rangle\langle i|], \quad (1)$$

where ϵ_i is the on-site potential at the ith site and has a value ϵ_A or ϵ_B depending on whether it is an edge site or a bulk one. The uniform nearest-neighbor hopping amplitude is $t_{ij} = t$ along the edges and $t_{ij} = \lambda$ when i and j refer to opposite vertices, connected by a diagonal. Thus we keep the provision of including hopping beyond the nearest neighbors. θ_{ij} is the Peierls phase,[42] given by $\theta_{ij} = 2\pi\,\Phi/4\Phi_0$ for hopping along an edge. $\Phi_0 = hc/e$ is the fundamental flux quantum. From symmetry considerations, $\theta_{ij} = 0$ when the electron hops across a diagonal, that is, when $t_{ij} = \lambda$.

B. The RSRG scheme

An elegant way of handling such self-similar systems is to use the RSRG method[43] where one can decimate out a subset of atomic sites from the original lattice to get a scaled version of it [Fig. 1(b)]. This is easily done by writing down in detail

the set of difference equations,

$$(E-\epsilon_i)\,\psi_i = \sum_j t_{ij} e^{i\theta_{ij}}\,\psi_j, \tag{2}$$

where ψ_i denotes the amplitude of the wave function at the ith site and θ_{ij} is the Peierls phase associated with the hopping matrix element connecting the ith and the jth sites. We begin with nearest-neighbor hopping only (that is, we set $\lambda = 0$ at the beginning). However, such a decimation automatically generates the next-nearest-neighbor hopping across the diagonals of an inflated diamond, as shown by the dotted lines in Fig. 1(b). The range of interactions, of course, does not increase beyond this on further renormalization. It is therefore advisable to retain λ in the Hamiltonian from the very beginning. One can easily compare the results obtained by switching λ on or off. The recursion relations of the on-site potentials and the hopping integrals are provided below.

$$\begin{aligned}
\epsilon_A' &= \epsilon_A + [pt_f + p^* t_b + \alpha\lambda_1],\\
\epsilon_B' &= \epsilon_B + 2\,[pt_f + p^* t_b + \alpha\lambda_1],\\
t_f' &= \beta\lambda_1, \quad t_b' = \beta^*\lambda_1, \quad \lambda' = \gamma\lambda_1,
\end{aligned} \tag{3}$$

where $\alpha = [(E-\bar{\epsilon}_B)\lambda_1]/\xi_3$, $\beta = [(E-\bar{\epsilon}_B)\bar{t}_f + \lambda_2\bar{t}_b]/\xi_3$, $\beta^* = [(E-\bar{\epsilon}_B)\bar{t}_b + \lambda_2\bar{t}_f]/\xi_3$, $\gamma = \lambda_1\lambda_2/\xi_3$, $\xi_3 = (E-\bar{\epsilon}_B)^2 - \lambda_2^2$, with $\bar{\epsilon}_B = \tilde{\epsilon}_B + w^* t_f + w t_b$, $\bar{t}_f = u t_f + v t_b$, $\bar{t}_b = v t_f + u t_b$, $\lambda_2 = \lambda + w t_f + w^* t_b$. Here $u = [(E-\tilde{\epsilon}_B)\lambda_1]/\xi_2$, $v = \lambda\lambda_1/\xi_2$, $w = [(E-\tilde{\epsilon}_B)t_f + \lambda t_b]/\xi_2$, $w^* = [(E-\tilde{\epsilon}_B)t_b + \lambda t_f]/\xi_2$, $\xi_2 = (E-\tilde{\epsilon}_B)^2 - \lambda^2$, with $\tilde{\epsilon}_B = \epsilon_B + pt_f + p^* t_b$, $\lambda_1 = \lambda + p^* t_f + p t_b$, and $p = [(E-\epsilon_A)t_b + \lambda t_f]/\xi_1$, $p^* = [(E-\epsilon_A)t_f + \lambda t_b]/\xi_1$, $\xi_1 = (E-\epsilon_A)^2 - \lambda^2$. In the above expression, $t_f = t_b^* = te^{i\theta}$, where $\theta = 2\pi\Phi/4\Phi_0$ is the constant Peierls phase. The above recursion relations are then used to obtain information about the local density of states (LDOS) at specific sites of the system and the character of the single-particle states, as discussed below.

III. SPECTRAL PROPERTIES WITH ZERO MAGNETIC FIELD

A. Local density of states in zero magnetic field and with $\lambda = 0$

Using the standard decimation procedure,[43] the LDOS at the edge (A) and the bulk (B) sites can easily be obtained through the local Green's functions. For simplicity we present in Fig. 2(a) the LDOS at a B site only, given by

$$\rho^{(B)}(E) = \lim_{\eta\to 0}\left[-\frac{1}{\pi}\,\mathrm{Im}\,\{G^{(B)}(E+i\eta)\}\right], \tag{4}$$

where $G^{(B)}(E+i\eta) = (E+i\eta-\epsilon_B^*)^{-1}$, with ϵ_B^* being the fixed point value of the relevant on-site potential at the B site, obtained by iterating Eq. (3). We have set $\epsilon_A = \epsilon_B = 0$, $t = 1$, and $\lambda = 0$, and there is no magnetic field (i.e., $\Phi = 0$). The LDOS shows a dense packing of eigenstates over a finite range of energy centered at $E = 0$. We have minutely examined this continuum by finely scanning an energy interval around $E = 0$, and we show it in Fig. 2(b). The continuum seems to persist. In the neighborhood of the band center and within the apparent "continuum," the hopping integral remains nonzero over a substantial number of RSRG iteration steps.

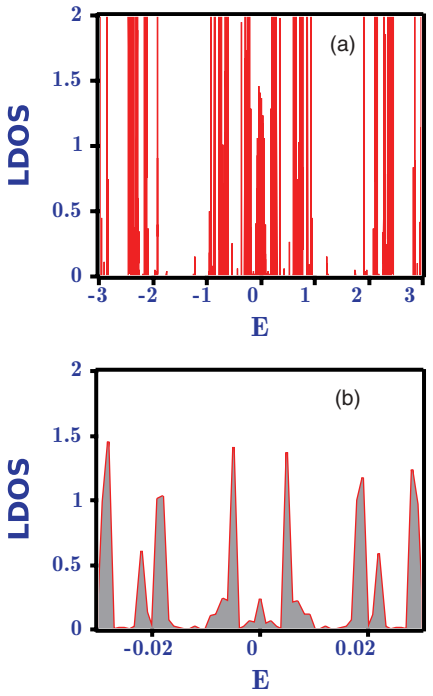

FIG. 2. (Color online) (a) LDOS versus E plot at the bulk sites (B type) of an infinite diamond-Vicsek network in the absence of the magnetic field ($\Phi = 0$). The other parameters are $\epsilon_A = \epsilon_B = 0$, $t = 1$, and $\lambda = 0$. (b) A highlighted version of (a) around the center $E = 0$. Energy, in units of t, is scanned in an interval of 0.001, and the imaginary part η has been chosen as 10^{-5}.

In addition to the band center, similar clusterings of states are observed in other parts of the spectrum as well. A finer scan of the energy interval in all such cases reveals similar dense clustering and apparent continua of states. The hopping integrals in all such intervals survive for quite a number of RSRG steps. The number of such steps n depends on the chosen energy and indicates that the corresponding eigenfunction is either of an *extended* character or, at least, has a very large localization length. This aspect will be further discussed in the following section in relation to the so-called staggered localization effect.

A particularly interesting state is the band center, viz., $E = 0$, where the entire parameter space $\{\epsilon_A,\epsilon_B,t,\lambda\}$ exhibits a one-cycle *fixed-point* behavior, viz., $\{\epsilon_A(n+1),\epsilon_B(n+1),t(n+1),\lambda(n+1)\} = \{\epsilon_A(n),\epsilon_B(n),t(n),\lambda(n)\}$ for $n \geqslant 1$, where n stands for the RSRG iteration step. λ at this special energy remains zero throughout the iteration. We conclude that the eigenstate at the band center is definitely extended, but it is of a non-Bloch character. The general behavior of the hopping integrals under successive RSRG iterations is suggestive of the fact that this central extended eigenstate might be flanked on either side by a countable infinity of eigenstates which either belong to the extended category or have very large localization lengths.

B. Exact construction of eigenstates

The inherent self-similarity of the deterministic fractals allows for the construction of the exact distribution of

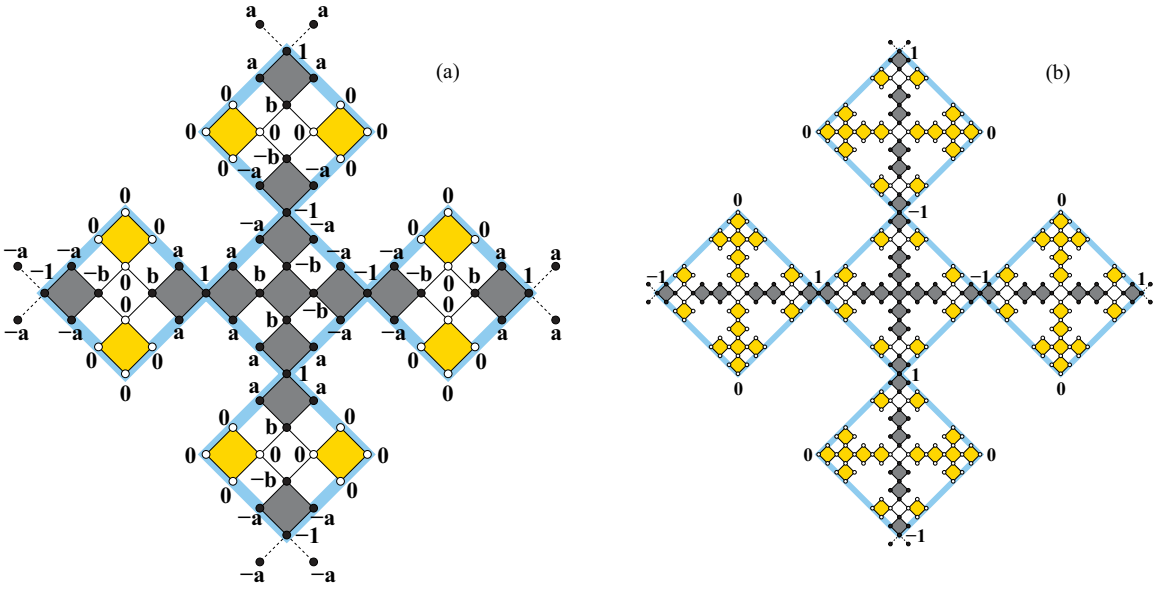

FIG. 3. (Color online) (a) Distribution of amplitudes of the wave functions at $E = \sqrt{6}$ [obtained by solving Eq. (5) for $n = 1$] on a second-generation lattice. The dark gray shaded plaquettes embrace atomic sites with nonzero amplitudes (solid circles), and the light yellow shaded plaquettes are surrounded by atomic sites with zero amplitudes (open circles). The initial parameters are chosen as $\Phi = 0, \epsilon_A = \epsilon_B = 0$, $t = 1$, and $\lambda = 0$. Here $a = \sqrt{6}/4$ and $b = 1/2$. (b) Distribution of amplitudes of the wave functions at $E = \sqrt{6}$ on a third-generation lattice; the other parameters and symbols are the same as in (a). In (a) and (b), the highlighted thick blue lines represent one-step and two-step renormalized lattices, respectively.

amplitudes of the eigenstates by suitably exploiting Eq. (2). Previous attempts in this regard have unfolded extended non-Bloch states (*atypically extended* states) in the cases of an open-loop Vicsek fractal[44] or a closed-loop diamond hierarchical geometry.[45] The present lattice offers a richer spectrum, allowing one to explicitly construct localized states extending over clusters of lattice points of various sizes on the parent lattice. The planar extent of such clusters depends on the eigenvalue corresponding to the localized state and can be small or enormous.

To elaborate, let us consider the solutions of the equation

$$E = \epsilon_B(n) - 2\lambda(n), \tag{5}$$

where n refers to the stage of renormalization. This is, in general, a polynomial equation in E. The zeroes of the polynomial will be eigenvalues of the infinite system if and only if one can use them to satisfy Eq. (2) locally at every vertex of the lattice, even when the lattice grows infinitely large. This task can be accomplished by trying to draw a nontrivial distribution of amplitudes for an energy obtained from Eq. (5) on the undecimated vertices of an n-step renormalized lattice and then trying to figure out the amplitude distribution on the original lattice at the bare length scale. Let us discuss two specific cases.

Case I. We begin with the unrenormalized lattice. Now $n = 0$, and with $\epsilon_A = \epsilon_B = 0$ and $\lambda = 0$ the solution of Eq. (5) is $E = 0$. One can construct an eigenfunction for $E = 0$ with amplitudes equal to ± 1 distributed alternately at the B sites along the major X and Y axes. The difference equation [Eq. (2)] can then easily be satisfied for all other intermediate vertices using the values 0 or ± 1.

Case II. The above idea can indeed be extended to higher values of n, as we demonstrate in Fig. 3(a) for $n = 1$ and discuss below. Let us extract the roots of Eq. (5) for $n = 1$. The roots are $E = 0$ and $\pm\sqrt{6}$ for $\epsilon_A = \epsilon_B = 0$, $t = 1$, and $\lambda = 0$ initially. We explain the construction of amplitudes for $E = \sqrt{6}$. The trick in this case is to place the values ± 1 periodically along the major X and Y axes and to assign an amplitude equal to *zero* at every edge (A-type site) on a *one-step renormalized* lattice. The amplitudes at the intermediate sites of the original lattice are then systematically evaluated using Eq. (2). We show distribution of amplitudes in Fig. 3(a) on a small portion of an infinite lattice. The larger square boxes with thick highlighted edges represent the one-step renormalized lattice. The construction depicted on a smaller scale can be extended to see that the distribution holds on a lattice of larger spatial extent [Fig. 3(b)]. In fact it holds even on a lattice of an arbitrarily large size, where the *end* sites are not actually visible. As, according to our earlier argument, we are able to satisfy Eq. (2) locally at every vertex while drawing this distribution, $E = \sqrt{6}$ is definitely an eigenvalue of the infinite system, a fact that has been cross-checked by evaluating the LDOS at the A and B sites at this special energy. We get a stable, finite value of the LDOS which supports our argument above.

Looking back at Fig. 3, the solid circles represent nonzero values of the amplitude, while open circles represent an amplitude equal to zero. Nonzero amplitudes, represented by the solid circles, have values equal to $\pm 1, \pm\sqrt{6}/4$ (depicted by the letter a), and $\pm 1/2$ (depicted by b), distributed suitably so as satisfy Eq. (2) consistently at every intermediate vertex on the original lattice. The gray shaded clusters in Fig. 3(a) embrace the nonzero amplitudes only, while every yellow shaded zone

is surrounded by vertices where amplitudes are zero. The significant observation is that clusters of nonzero amplitude span over a finite distance but ultimately get decoupled from each other on a larger scale of length. This can be appreciated if we look at Fig. 3(b), which is a larger version of Fig. 3(a). The gray shaded clusters are distributed along the principal X and Y axes but are *decoupled* from each other beyond a certain extent by the unfilled white boxes. The yellow clusters representing amplitude voids are now seen to span larger spatial distances. A similar construction is possible for $E = -\sqrt{6}$, which is another solution of Eq. (5) for $n = 1$.

C. Staggered localization

It is apparent from the above discussion that the eigenfunction corresponding to $E = \pm\sqrt{6}$ will be localized in the fractal space, as the spanning clusters of different sizes and embracing nonzero amplitudes ultimately get decoupled from one another. This is easily reconfirmed by studying the evolution of the hopping integrals under successive RSRG steps. The hopping integrals t and λ (zero initially but grows later) remain nonzero at the first stage of RSRG (that is, $n = 1$), indicating that the nearest-neighbor sites on a one-step renormalized lattice will have a nonzero overlap of the eigenfunctions. They start decaying for $n \geqslant 2$ with the decay in $\lambda(n)$ taking place at a much slower rate compared to $t(n)$. This indicates that over a larger scale of length the corresponding states are ultimately *localized*, but the effect is a weak one.

This observation immediately leads to an innovative way of exactly determining a localized eigenstate on such a deterministic geometry. It should be appreciated that although it is not unnatural that most of the single-particle states will be Anderson localized in the absence of any translational order, an exact prescription of the determination of any localized eigenvalue is not easy to obtain and has not been reported so far in the literature to the best of our knowledge. We do it using the following method.

We can solve Eq. (5), in principle, for any n. For example, we have done it explicitly for $n = 1$, $n = 2$, $n = 3$, and $n = 4$. With the same set of parameters as discussed above, the roots of Eq. (5) for $n = 2$ are $E = 0, \pm\sqrt{6}, \pm 2.11619, \pm 0.77508, \pm 2.98681$. As we observe, the roots for the $n = 1$ stage, viz., $E = 0$ and $\pm\sqrt{6}$, are included in this set for $n = 2$. $E = 0$ corresponds to the extended state, and $E = \pm\sqrt{6}$ provide two localized states we already know. For each of the additional roots, viz., $E = \pm 2.11619, \pm 0.77508, \pm 2.98681$, the hopping integrals t and λ remain nonzero (with considerable magnitude) up to the second stage of iteration ($n = 2$) and start to lose their "strengths" as the renormalization progresses. Finally, for large n the hopping integrals become zero.

The above observation implies that, using a subset of energy values extracted at the stage $n = 2$ ($E = \pm 2.11619, \pm 0.77508$, and ± 2.98681), we can work out eigenfunctions which will span bigger clusters of lattice points on the original lattice compared to those obtained from $n = 1$. The states will appear to be "extended" when viewed on a finite diamond-Vicsek fractal at the second generation but will eventually be localized on a lattice in the thermodynamic limit. In Fig. 4 we show the distribution of amplitudes for $E = 0.77508$, a

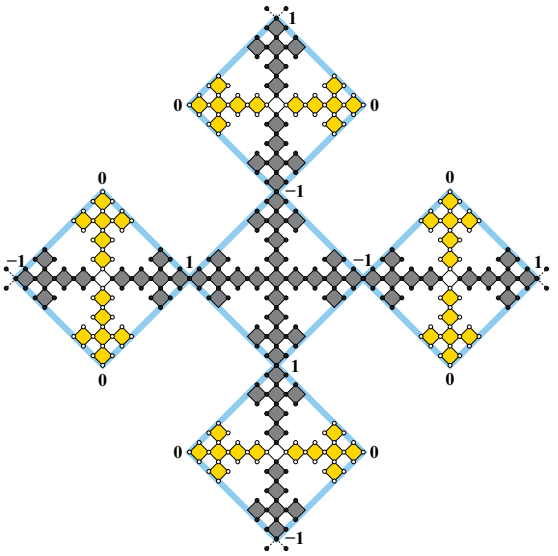

FIG. 4. (Color online) Distribution of amplitudes of the wave functions at $E = 0.77508$ [obtained by solving Eq. (5) for $n = 2$] on a third-generation lattice. The other parameters and symbols are the same as in Fig. 3. The thick highlighted blue lines represent a two-step renormalized lattice.

value that is obtained from Eq. (5) for $n = 2$. The enlargement in the cluster size having nonzero values of the amplitude in comparison to the $n = 1$ case [Fig. 3(b)] is obvious. The spanning clusters finally get decoupled from each other, just as occurred for the $n = 1$ case. But now this decoupling occurs at a larger length scale.

It is now easy to foresee what is going to happen for $n = 3, 4$ and beyond. For any $n = \ell$ we will be getting roots of Eq. (5), subsets of which are solutions of Eq. (5) for $n = 1, 2, \ldots, \ell - 1$. For these subsets, the decay in the hopping integrals will begin at $n > 1$, $n > 2$, $\ldots$, $n > \ell - 1$. For the roots in addition to these, the hopping integrals lose their strengths and finally decay, from $n > \ell$. Thus, the latter eigenvalues will correspond to localized eigenstates, the localization being *delayed* (staggered) in space with localization lengths much larger than the previous ones. When mapped back on to the original lattice, the amplitudes for these additional roots will be found to span clusters of increasing size. The exact size of the spanning clusters will be determined by the value of n.

The roots of Eq. (5) are found to cluster symmetrically around the value $E = 0$ and tend to densely fill the neighborhood of $E = 0$, at which the single extended eigenstate determined so far resides. The clustering of the eigenvalues is shown in Fig. 5. This dense filling of the eigenvalue spectrum around the center is also reflected in the apparent continuum observed in the density of states [Fig. 2(b)].

Before we end this section, we would like to point out that by the method of exact construction we have been able to identify a class of localized (staggered) eigenfunctions. This, of course, does not imply that all localized eigenstates have been exhausted in the present method. For example, looking back to Fig. 2(a) one can observe clusters of eigenstates even far away from the band center. If any energy picked up from such a cluster becomes a solution of Eq. (5) for some value of n, then such an energy will definitely correspond

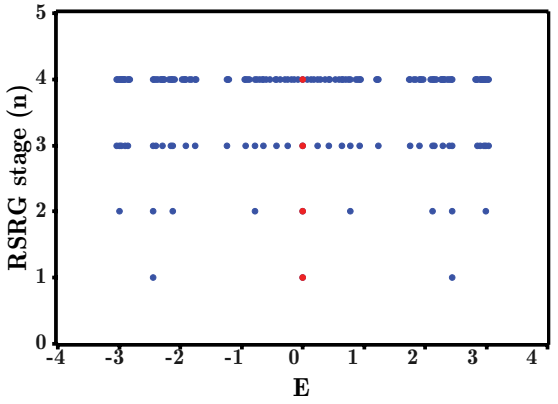

FIG. 5. (Color online) Distribution of energy eigenvalues E obtained from Eq. (5) for different RSRG stages n. The central red dot at $E = 0$ represents the eigenvalue for the extended eigenstate.

to a staggered localized eigenstate in the spirit of the above discussion. On examining the nesting property of the roots of Eq. (5) for several values of n, we should say that this indeed is a possibility.

IV. SPECTRAL PROPERTIES WITH NONZERO MAGNETIC FIELD

A. The energy eigenvalue spectrum

We have obtained the energy eigenvalue distribution (Fig. 6) as a function of the magnetic flux Φ enclosed in each basic plaquette for an infinite-size diamond-Vicsek fractal. We have examined the formation of the bands and the gaps with the variation of magnetic flux Φ. To obtain the energy spectrum, we have calculated the LDOS at both A and B sites by fixing the value of the energy E and varying the magnetic flux Φ from -1 to 1, repeated the above process for different values of energy E, and recorded those values of energy E and magnetic

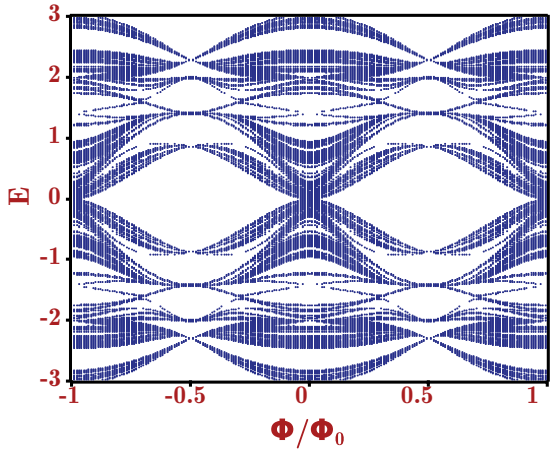

FIG. 6. (Color online) Energy eigenvalue spectrum of an infinite diamond-Vicsek fractal as a function of the magnetic flux Φ. We have chosen $\epsilon_A = \epsilon_B = 0$, $t = 1$, and $\lambda = 0$. At $\Phi = \Phi_0/2$, the bands touch each other only at $E = \pm 2$ and at $E = \pm\sqrt{2}$. The precise detection of these four energy values may be restricted here due to the limit of resolution.

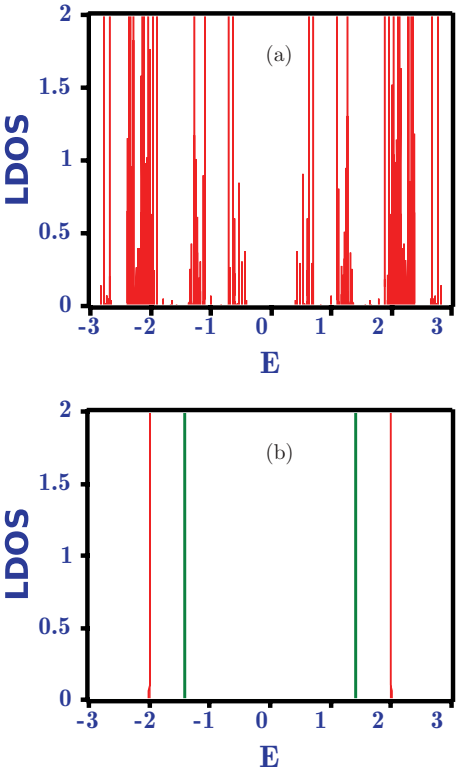

FIG. 7. (Color online) LDOS versus E plot at the bulk sites (B type) of an infinite diamond-Vicsek network (a) with $\Phi = \Phi_0/4$ and (b) with $\Phi = \Phi_0/2$. The red lines correspond to the LDOS at B sites, and the green lines correspond to the LDOS at A sites. We have chosen $\epsilon_A = \epsilon_B = 0$, $t = 1$, and $\lambda = 0$.

flux Φ for which we get a nonzero LDOS either at an A site or a B site. Thus Fig. 6 is representative of an infinite lattice.

In Fig. 6, we can clearly observe the formation of multiple bands and gaps and how a variation of magnetic flux Φ leads to band overlapping. The band crossing is maximum at the center (around $\Phi = 0$), and the density of allowed energy eigenvalues is large in this area. As we shift from $\Phi = 0$ on either side, there is thinning of the allowed energy eigenvalues. Finally, at $\Phi = \Phi_0/2$, only four energy eigenvalues are allowed, indicating an extreme localization of the electronic states, which is discussed in detail in the next section. Figure 6 confirms this last observation. At $\Phi = \Phi_0/2$, there are exactly four points at which the bands touch each other, although due to limit of resolution of the diagram, it may appear to be more. This is clearly resolved in Fig. 7(b).

B. Extreme localization of the electronic states

In the absence of magnetic field, there was clearly a nonzero value of the LDOS at the center of the spectrum (around $E = 0$) [Fig. 2(a)]. As soon as the magnetic field is switched on, a wide gap opens up in the LDOS spectrum around $E = 0$ [Fig. 7(a)]. The gap becomes wider as we increase the value of the magnetic flux Φ, finally leading to an extreme localization of electronic states [Fig. 7(b)] at the half flux quantum (i.e., $\Phi = \Phi_0/2$). The four separate lines in Fig. 7(b) (at $E = \pm\sqrt{2}$ and at $E = \pm 2$) correspond to four highly degenerate localized states pinned at the A and

B sites, respectively. This observation is in accordance with Vidal *et al.*'s result,[41] where the Aharonov-Bohm caging of the localized orbitals under the action of an external magnetic field was discussed.

The origin of the four localized-state eigenvalues above can be easily explained if one appreciates that at $\Phi = \Phi_0/2$, the effective coupling between the sites at the vertices of an elementary rhombus, viz., $t^{\rm eff} = [2t^2/(E-\epsilon_A)]\cos(\pi\Phi/\Phi_0)$, becomes equal to zero. In that case one is left with only two types of atomic sites, decoupled from each other and having effective on-site potential energies

$$\epsilon_A^{\rm eff} = \epsilon_A + \frac{2t^2}{E-\epsilon_B}, \qquad \epsilon_B^{\rm eff} = \epsilon_B + \frac{4t^2}{E-\epsilon_A} \tag{6}$$

for the edge and the bulk sites, respectively. With $\epsilon_A = \epsilon_B = 0$ and $t = 1$, the localized states are obtained by setting $E = \epsilon_A^{\rm eff}$ and $E = \epsilon_B^{\rm eff}$, which yield the values $E = \pm\sqrt{2}$ and ± 2, respectively. These are the energy eigenvalues at which extreme localization is observed, as shown in Fig. 7(b).

V. TWO-TERMINAL CONDUCTANCE FOR A FINITE LATTICE

To get the two-terminal conductance for a finite-size diamond-Vicsek fractal, we attach the system between two semi-infinite one-dimensional ordered metallic leads, namely, the source and the drain. The leads, in the tight-binding model, are described by a constant on-site potential ϵ_l and a nearest-neighbor hopping integral t_l. We then successively renormalize the system to reduce it to an effective diatomic system,[44] consisting of two "renormalized" atoms, each having an effective on-site potential equal to U and with an effective hopping integral V between them. The transmission coefficient across the effective dimer is given by the following well-known formula:[46]

$$T = \frac{4\sin^2 ka}{[(M_{12}-M_{21}) + (M_{11}-M_{22})\cos ka]^2 + [(M_{11}+M_{22})\sin ka]^2}, \tag{7}$$

where $M_{11} = \frac{(E-U)^2}{Vt_l} - \frac{V}{t_l}$, $M_{12} = -\frac{(E-U)}{V}$, $M_{21} = -M_{12}$, and $M_{22} = -\frac{t_l}{V}$ are the matrix elements of the transfer matrix for the effective diatomic system and $\cos ka = (E-\epsilon_l)/2t_l$, with a being the lattice constant, which is taken to be equal to unity throughout the calculation.

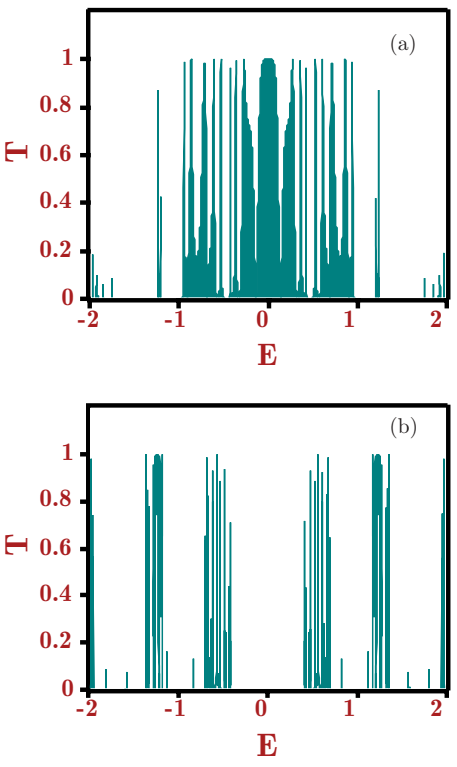

FIG. 8. (Color online) Transmission characteristics for a third-generation system for (a) $\Phi = 0$ and (b) $\Phi = \Phi_0/4$. The other parameters are $\epsilon_A = \epsilon_B = 0$, $t = 1$, and $\lambda = 0$. The lead parameters are $\epsilon_l = 0$ and $t_l = 1$.

In Fig. 8, we show the two-terminal transmission characteristics for a third-generation system for different values of magnetic flux Φ. For $\Phi = 0$, the system exhibits a continuous high-transmission window over a region at the center [Fig. 8(a)].

This is due to the fact that, on either side of $E = 0$, the energy eigenvalues become quite densely packed. The corresponding eigenfunctions have localization lengths extending much beyond the third-generation fractal.

As we tune the magnetic flux to a nonzero value, e.g., $\Phi = \Phi_0/4$, the transmission coefficient of the system drastically decreases [Fig. 8(b)], and with an increase in Φ, the value of the transmission coefficient T decreases more and more, and finally, at $\Phi = \Phi_0/2$, the system becomes completely opaque to an incoming electron. So by fixing the Fermi level of the electron to a particular energy, say at $E = 0$, one can easily transform the system from a conducting one to an insulating one by tuning the external magnetic flux Φ suitably.

VI. CONCLUDING REMARKS

In conclusion, we have examined the energy spectrum of a Vicsek geometry consisting of diamond-shaped loops. The major result is that we have been able to identify a countable infinity of localized eigenstates displaying a multitude of localization lengths. A prescription is given for an exact determination of the eigenvalues corresponding to all such states, a problem that is far from trivial in the case of an aperiodically ordered system. The localized states span across the fractal space in clusters of increasing sizes, with the size

being precisely controlled by the length scale at which the energy eigenvalue is extracted. The onset of localization can be exactly predicted from the stage of RSRG. In addition, the application of a uniform magnetic field perpendicular to the plane of the fractal is found to produce gaps in the energy spectrum. A special value of the magnetic flux, viz., $\Phi = \Phi_0/2$, is shown to lead to an extreme localization of the electron states as well. The results are corroborated by the density of states calculations and the valuation two-terminal magnetotransport.

ACKNOWLEDGMENTS

Biplab Pal would like to thank DST-INSPIRE Program, India, for providing financial assistance through an INSPIRE Fellowship (IF110078). Illuminating conversations with Bibhas Bhattacharyya are gratefully acknowledged.

*arunava_chakrabarti@yahoo.co.in

[1] P. W. Anderson, Phys. Rev. **109**, 1492 (1958).
[2] E. Abrahams, P. W. Anderson, D. C. Licciardello, and T. V. Ramakrishnan, Phys. Rev. Lett. **42**, 673 (1979).
[3] A. MacKinnon and B. Kramer, Phys. Rev. Lett. **49**, 695 (1982).
[4] D. J. Thouless, Phys. Rev. Lett. **61**, 2141 (1988).
[5] I. V. Plyushchay, R. A. Römer, and M. Schreiber, Phys. Rev. B **68**, 064201 (2003).
[6] A. Rodriguez, L. J. Vasquez, K. Slevin, and R. A. Römer, Phys. Rev. Lett. **105**, 046403 (2010).
[7] A. Rodriguez, L. J. Vasquez, K. Slevin, and R. A. Römer, Phys. Rev. B **84**, 134209 (2011).
[8] M. Zilly, O. Ujsághy, M. Woelki, and D. E. Wolf, Phys. Rev. B **85**, 075110 (2012).
[9] D. M. Jović, M. R. Belić, and C. Denz, Phys. Rev. A **85**, 031801 (2012).
[10] K. Y. Bliokh, S. A. Gredeskul, P. Rajan, I. V. Shadrivov, and Y. S. Kivshar, Phys. Rev. B **85**, 014205 (2012).
[11] C. Echeverria-Arrondo and E. Ya. Sherman, Phys. Rev. B **85**, 085430 (2012).
[12] T. A. Sedrakyan, J. P. Kestner, and S. Das Sarma, Phys. Rev. A **84**, 053621 (2011).
[13] S. Aubry and G. André, Ann. Israel Phys. Soc. **3**, 133 (1980).
[14] S. Das Sarma, S. He, and X. C. Xie, Phys. Rev. B **41**, 5544 (1990).
[15] J. Billy, V. Josse, Z. Zuo, A. Bernard, B. Hambrecht, P. Lugan, D. Clément, L. Sanchez-Palencia, P. Bouyer, and A. Aspect, Nature (London) **453**, 891 (2008).
[16] E. E. Edwards, M. Beeler, T. Hong, and S. L. Rolston, Phys. Rev. Lett. **101**, 260402 (2008).
[17] G. Roati, C. D'Errico, L. Fallani, M. Fattori, C. Fort, M. Zacanti, G. Modugno, M. Modugno, and M. Inguscio, Nature (London) **453**, 895 (2008).
[18] Z. Shi and A. Z. Genack, Phys. Rev. Lett. **108**, 043901 (2012).
[19] A. A. Asatryan, L. C. Botten, M. A. Byrne, V. D. Freilikher, S. A. Gredeskul, I. V. Shadrivov, R. C. McPhedran, and Y. S. Kivshar, Phys. Rev. B **85**, 045122 (2012).
[20] D. H. Dunlap, H.-L. Wu, and P. W. Phillips, Phys. Rev. Lett. **65**, 88 (1990); D. H. Dunlap, K. Kundu, and P. W. Phillips, Phys. Rev. B **40**, 10999 (1989).
[21] F. A. B. F. de Moura and M. L. Lyra, Phys. Rev. Lett. **81**, 3735 (1998).
[22] A. Sánchez, E. Maciá, and F. Domínguez-Adame, Phys. Rev. B **49**, 147 (1994).
[23] A. Chakrabarti, S. N. Karmakar, and R. K. Moitra, Phys. Rev. Lett. **74**, 1403 (1995).
[24] A. Chakrabarti, S. N. Karmakar, and R. K. Moitra, Phys. Rev. B **50**, 13276 (1994).
[25] E. Maciá and F. Domínguez-Adame, Phys. Rev. Lett. **76**, 2957 (1996).
[26] E. Maciá, Phys. Rev. B **60**, 10032 (1999).
[27] E. Maciá, *Aperiodic Structures in Condensed Matter* (CRC Press, Boca Raton, FL, 2009).
[28] A. Chakrabarti, J. Phys. Condens. Matter **8**, 10951 (1996).
[29] A. Chakrabarti, Phys. Rev. B **72**, 134207 (2005).
[30] W. A. Schwalm and B. J. Moritz, Phys. Rev. B **71**, 134207 (2005).
[31] S. Sil, S. K. Maiti, and A. Chakrabarti, Phys. Rev. Lett. **101**, 076803 (2008).
[32] F. A. B. F. de Moura, R. A. Caetano, and M. L. Lyra, Phys. Rev. B **81**, 125104 (2010).
[33] T. Vicsek, *Fractal Growth Phenomena*, 2nd ed. (World Scientific, Singapore, 1992).
[34] R. Rammal and G. Toulouse, Phys. Rev. Lett. **49**, 1194 (1982).
[35] E. Domany, S. Alexander, D. Bensimon, and L. P. Kadanoff, Phys. Rev. B **28**, 3110 (1983).
[36] Y. Lin, B. Wu, and Z. Zhang, Phys. Rev. E **82**, 031140 (2010).
[37] C. S. Jayanthi and S. Y. Wu, Phys. Rev. B **48**, 10188 (1993).
[38] S. Sil, S. K. Maiti, and A. Chakrabarti, Phys. Rev. B **79**, 193309 (2009).
[39] A. Aharony, O. Entin-Wohlman, Y. Tokura, and S. Katsumoto, Phys. Rev. B **78**, 125328 (2008).
[40] A. Aharony, O. Entin-Wohlman, Y. Tokura, and S. Katsumoto, Phys. E **42**, 629 (2010).
[41] J. Vidal, R. Mosseri, and B. Doucot, Phys. Rev. Lett. **81**, 5888 (1998).
[42] R. Peierls, Z. Phys. **80**, 763 (1933).
[43] B. W. Southern, A. A. Kumar, and J. A. Ashraff, Phys. Rev. B **28**, 1785 (1983).
[44] A. Chakrabarti and B. Bhattacharyya, Phys. Rev. B **54**, R12625 (1996).
[45] A. Chakraborti, B. Bhattacharyya, and A. Chakrabarti, Phys. Rev. B **61**, 7395 (2000).
[46] A. D. Stone, J. D. Joannopoulos, and D. J. Chadi, Phys. Rev. B **24**, 5583 (1981).